





Band-folding-driven high tunnel magnetoresistance ratios in (111)-oriented junctions with SrTiO₃ barriers

Keisuke Masuda ^{1,*}, Hiroyoshi Itoh ^{2,3}, Yoshiaki Sonobe,⁴ Hiroaki Sukegawa ¹, Seiji Mitani,^{1,5} and Yoshio Miura ^{1,3}

¹Research Center for Magnetic and Spintronic Materials, National Institute for Materials Science (NIMS), Tsukuba 305-0047, Japan

²Department of Pure and Applied Physics, Kansai University, Suita 564-8680, Japan

³Center for Spintronics Research Network, Osaka University, Toyonaka 560-8531, Japan

⁴Research Organization for Nano & Life Innovation, Waseda University, Shinjuku 162-0041, Japan

⁵Graduate School of Science and Technology, University of Tsukuba, Tsukuba 305-8577, Japan



(Received 14 September 2022; accepted 18 October 2022; published 31 October 2022)

We theoretically study the tunnel magnetoresistance (TMR) effect in (111)-oriented magnetic tunnel junctions (MTJs) with SrTiO₃ barriers, Co/SrTiO₃/Co(111) and Ni/SrTiO₃/Ni(111). Our analysis combining the first-principles calculation and the Landauer formula shows that the Co-based MTJ has a high TMR ratio over 500%, while the Ni-based MTJ has a smaller value (290%). Since the in-plane lattice periodicity of SrTiO₃ is about twice that of the primitive cell of fcc Co (Ni), the original bands of Co (Ni) are folded in the k_x - k_y plane corresponding to the ab plane of the MTJ supercell. We find that this band folding gives a half-metallic band structure in the Δ_1 state of Co (Ni) and the coherent tunneling of such a half-metallic Δ_1 state yields a high TMR ratio. We also reveal that the difference in the TMR ratio between the Co- and Ni-based MTJs can be understood by different s -orbital weights in the Δ_1 band at the Fermi level.

DOI: [10.1103/PhysRevB.106.134438](https://doi.org/10.1103/PhysRevB.106.134438)

I. INTRODUCTION

The tunnel magnetoresistance (TMR) effect is essential not only for applications to magnetic sensors and memories but also for deepening our understanding of spin-dependent electron transport. A series of studies on Fe/MgO/Fe(001) magnetic tunnel junctions (MTJs) [1–4] has established the so-called coherent tunneling mechanism, which explains the TMR effect by bulk band structures of bcc Fe and MgO. In the Δ line of the Brillouin zone corresponding to the [001] direction, MgO has the slowest-decaying evanescent state with Δ_1 symmetry within the band gap, allowing the major contribution of the Δ_1 wave function to the transmission. Since bcc Fe has a half-metallic band structure in the Δ_1 state, the majority-spin Δ_1 wave function can mainly tunnel through MgO, leading to a giant TMR effect. Because of the successful observation of high TMR ratios [3,4], this mechanism has been widely accepted and bcc(001)-oriented MTJs with MgO barriers have been mainly studied from both experimental and theoretical points of view.

In contrast, our recent studies [5,6] have focused on unconventional fcc(111)-oriented MTJs with the stacking direction parallel to [111] directions of both the fcc ferromagnetic electrode and the insulator barrier. These MTJs are advantageous for obtaining large perpendicular magnetic anisotropy (PMA), which is another requirement in addition to high TMR ratios for the application to magnetic random access memories. There are many fcc ferromagnetic materials with large magnetic anisotropy along their [111] directions. Moreover, the (111) plane of the fcc structure is the closed-packed plane and

has the lowest surface energy, indicating that (111)-oriented MTJs are compatible with fcc ferromagnetic electrodes. Thus we have investigated the potential of such MTJs in the TMR effect on the basis of the first-principles calculation. We have shown that several (111)-oriented MTJs with Co-based ferromagnetic electrodes and MgO barriers have high TMR ratios [5,6], which originate from the interfacial resonant tunneling, in contrast to the conventional coherent tunneling of bulk electronic states in ferromagnetic electrodes.

Although such a mechanism of high TMR ratios is physically significant, the interfacial resonant tunneling might be sensitive to atomic configurations at interfaces of MTJs. Moreover, the application of bias voltages tends to suppress the interfacial resonant tunneling, since the energy level of the interfacial state is shifted oppositely in the two interfaces. These motivate us to find other (111)-oriented MTJs with robustly high TMR ratios. In this work, we consider (111)-oriented MTJs with SrTiO₃ tunnel barriers. Historically, SrTiO₃ has been recognized as an important material for tunnel barriers. Comparative experimental studies on Co/ X /La_{0.7}Sr_{0.3}MnO₃ ($X = \text{SrTiO}_3, \text{Al}_2\text{O}_3$, and Ce_{0.69}La_{0.31}O_{1.845}) clarified that the spin polarization of effective tunneling electrons but not that of ferromagnets plays a crucial role in the TMR effect [7,8]. Moreover, a high TMR ratio was predicted theoretically in bcc(001)-oriented Co/SrTiO₃/Co(001) [9]. Although experiments on such (001)-oriented MTJs have not succeeded in achieving high TMR ratios, unconventional (111)-oriented MTJs with SrTiO₃ barriers may open a pathway for high TMR ratios. We thus focus on fcc(111)-oriented MTJs, Co/SrTiO₃/Co(111) and Ni/SrTiO₃/Ni(111) (Fig. 1).

Our first-principles-based transport calculation demonstrates that the Co- and Ni-based MTJs show relatively high

*MASUDA.Keisuke@nims.go.jp

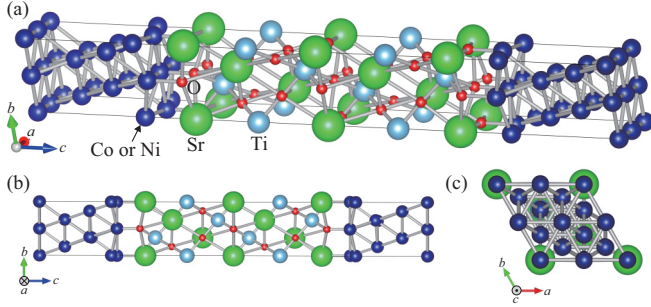


FIG. 1. Supercell of $X/\text{SrTiO}_3/X(111)$ ($X = \text{Co}$ or Ni). (a) Three-dimensional view. (b) Side view from the a -axis and (c) top view from the c -axis directions.

TMR ratios of 534 and 290%, respectively. We also reveal that the high TMR ratios can be explained by the coherent tunneling of electronic states of bulk ferromagnets, meaning that the obtained TMR ratios are more robust against interfacial imperfections and bias voltage than those driven by the interfacial resonant tunneling. The simple fcc Co and Ni given by their primitive unit cells have no Δ_1 bands crossing the Fermi level in the high-symmetry line Δ corresponding to the $[111]$ direction. We show however that these ferromagnets have a half-metallic band structure in the Δ_1 state when attached to SrTiO_3 , because the in-plane periodicity of SrTiO_3 is about twice that of fcc Co (or Ni) and the original band structure of Co (or Ni) is folded in the k_x - k_y plane. This is a kind of “band-folding effect” found and studied in (001)-oriented MTJs with spinel-oxide tunnel barriers [10–14]. Finally, we address the difference in the TMR ratio between the Co- and Ni-based MTJs and clarify that this comes from different s -orbital weights in the Δ_1 band at the Fermi level.

II. MODEL AND METHOD

We first considered supercells of $\text{Co}/\text{SrTiO}_3/\text{Co}(111)$ and $\text{Ni}/\text{SrTiO}_3/\text{Ni}(111)$ (Fig. 1), in which fcc Co (or Ni) and SrTiO_3 are stacked along their $[111]$ directions. These supercells have the hexagonal close-packed structure given by the primitive translation vectors, $\mathbf{a}_1 = a(1, 0, 0)$, $\mathbf{a}_2 = a(-1/2, \sqrt{3}/2, 0)$, and $\mathbf{a}_3 = (0, 0, c)$, where $a = \sqrt{2} a_{\text{fcc}}$ with a_{fcc} being the lattice constant of fcc Co (or Ni) and c is the length of the supercell. We used $a_{\text{fcc}} = 3.52 \text{ \AA}$ for both the supercells and fitted SrTiO_3 to fcc Co (or Ni) in the ab plane. The length c was determined by the structure optimization mentioned below. The supercell includes 13 monolayers (ML) of SrTiO_3 and 7 ML of Co (or Ni). The thickness of SrTiO_3 layers is approximately 1.9 nm [15], which is a typical barrier thickness (1–2 nm) used in MTJs. Note here that there are four possible candidates of the interfacial atomic configuration of the supercell as shown in Fig. 2. After preparing supercells for all the cases, atomic positions in each supercell were relaxed along the c direction and the formation energy of each supercell was calculated. To determine the energetically favored supercell, we compared formation energies of $\text{Co}/\text{SrTiO}_3/\text{Co}(111)$ supercells with different interfacial atomic configurations [Figs. 2(a)–2(d)]. The formation energy

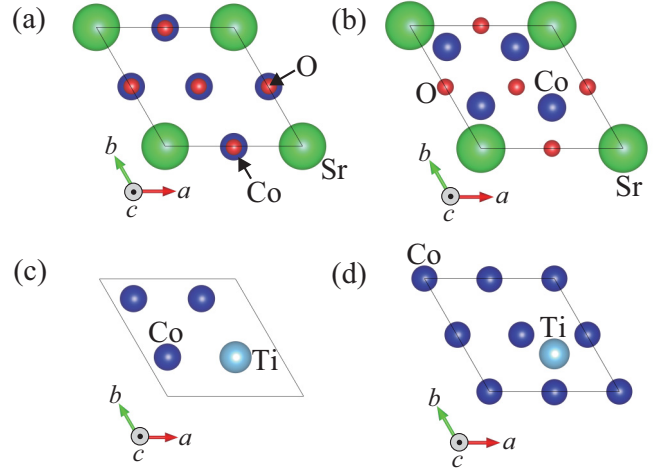


FIG. 2. Top view of different interfacial atomic configurations in $\text{Co}/\text{SrTiO}_3/\text{Co}(111)$. (a),(b) SrO-terminated interfaces with (a) Sr and O on top of Co and (b) Sr and O on hollow sites. (c),(d) Ti-terminated interfaces with (c) Ti on top of Co and (d) Ti on hollow sites.

for each supercell is expressed as

$$E_{\text{form}} = E_{\text{tot}} - \sum_i N_i \mu_i, \quad (1)$$

where E_{tot} is the total energy of the optimized supercell with each interfacial atomic configuration, N_i is the number of atoms of the element i and μ_i is its chemical potential. In the present work, we used μ_{Co} , μ_{Sr} , μ_{Ti} , and μ_{O} derived from energies of hcp Co, fcc Sr, hcp Ti, and O_2 molecules. Table I shows obtained formation energies. We find that the supercell with the SrO-terminated interface with Sr and O on top of Co [Fig. 2(a)] has the lowest value of E_{form}/V . Therefore, this supercell (Fig. 1) was selected for the calculation of the TMR ratio. All the structural optimizations were performed using the first-principles calculation based on the density-functional theory (DFT) implemented in the Vienna *ab initio* simulation program (VASP) [16]. We adopted the generalized gradient approximation (GGA) [17] for the exchange-correlation energy and used the projected augmented wave (PAW) pseudopotential [18,19] to treat the effect of core electrons properly. A cutoff energy of 500 eV was employed and the Brillouin-zone integration was performed with $13 \times 13 \times 1$ \mathbf{k} points. More details of the structural optimization are mentioned in our previous work [12].

We calculated the TMR ratios on the basis of the ballistic transport theory. The Landauer formula was used in

TABLE I. Formation energy divided by the cell volume E_{form}/V in each $\text{Co}/\text{SrTiO}_3/\text{Co}(111)$ supercell.

Interfacial atomic configuration	E_{form}/V (eV/Å ³)
Co-SrO (on top)	-1.899×10^{-1}
Co-SrO (hollow)	-1.878×10^{-1}
Co-Ti (hollow)	-1.513×10^{-1}
Co-Ti (on top)	-1.506×10^{-1}

TABLE II. Conductances per unit areas and TMR ratios calculated using supercells with 13 ML of SrTiO₃. The units are in $\Omega^{-1}\mu\text{m}^{-2}$ and %, respectively. Here, $A = 2.15 \times 10^{-7} \mu\text{m}^2$ is the in-plane area of both the supercells.

	Co/SrTiO ₃ /Co(111)	Ni/SrTiO ₃ /Ni(111)
$G_{P,\uparrow}/A$	2.78×10^{-3}	2.15×10^{-3}
$G_{P,\downarrow}/A$	1.51×10^{-1}	3.56×10^{-2}
$G_{AP,\uparrow}/A$	1.20×10^{-2}	4.85×10^{-3}
$G_{AP,\downarrow}/A$	1.22×10^{-2}	4.84×10^{-3}
G_P/A	1.53×10^{-1}	3.78×10^{-2}
G_{AP}/A	2.42×10^{-2}	9.68×10^{-3}
TMR ratio	534	290

ballistic transport calculations with the first-principles DFT method, which is implemented in the PWCOND code [20] in the QUANTUM ESPRESSO package [21]. We first constructed the quantum open system by attaching the left and right semi-infinite electrodes of fcc Co (Ni) to the supercell Co/SrTiO₃/Co (Ni/SrTiO₃/Ni). Then, the self-consistent potential of the quantum open system was obtained by the first-principles calculation, where the GGA and the ultrasoft pseudopotentials [22] were used. The cutoff energies for the wave functions and the charge density were fixed to 58 and 580 Ry, respectively, and $13 \times 13 \times 1$ \mathbf{k} points were used for the Brillouin-zone integration. Since the quantum open system has the translational symmetry in the ab plane, the scattering state can be classified by an in-plane wave vector $\mathbf{k}_{\parallel} = (k_x, k_y)$, where the x axis was set to be parallel to the a axis. Here, (x, y) and (k_x, k_y) are given in the Cartesian coordinates. For each \mathbf{k}_{\parallel} and spin index, we solved the scattering equation derived under the condition that the wave function and its derivative of the supercell are connected to those of the electrodes [20,23]. From the obtained transmittance, we calculated the conductance using the Landauer formula. These calculations for both parallel (P) and antiparallel (AP) magnetization states of electrodes provide the following wave-vector-resolved conductances: $G_{P,\uparrow}(\mathbf{k}_{\parallel})$, $G_{P,\downarrow}(\mathbf{k}_{\parallel})$, $G_{AP,\uparrow}(\mathbf{k}_{\parallel})$, and $G_{AP,\downarrow}(\mathbf{k}_{\parallel})$, where \uparrow (\downarrow) indicates the up-spin (down-spin) channel. In this work, the up-spin (down-spin) channel is defined as the majority-spin (minority-spin) channel of the left electrode in both the parallel and antiparallel magnetization states. We calculated the averaged conductances as, e.g., $G_{P,\uparrow} = \sum_{\mathbf{k}_{\parallel}} G_{P,\uparrow}(\mathbf{k}_{\parallel})/N$, where N is the sampling number of \mathbf{k}_{\parallel} points. After confirming good convergence of the conductances and TMR ratio, N was set to $150 \times 150 = 2250$. Using the averaged conductances, we calculated the TMR ratio given by the optimistic definition, i.e., $\text{TMR ratio (\%)} = 100 \times (G_P - G_{AP})/G_{AP}$, where $G_{P(AP)} = G_{P(AP),\uparrow} + G_{P(AP),\downarrow}$.

III. RESULTS AND DISCUSSION

Table II shows the obtained conductances and TMR ratios in Co/SrTiO₃/Co(111) and Ni/SrTiO₃/Ni(111) MTJs. The Co-based MTJ exhibits a relatively high TMR ratio over 500%, which is higher than that of the Ni-based MTJ (290%). Note that the down-spin conductance $G_{P,\downarrow}$ is much larger than the up-spin conductance $G_{P,\uparrow}$ in both MTJs. This is a

significant feature for the present TMR effect and its origin is discussed below.

In Fig. 3, we show the \mathbf{k}_{\parallel} -dependent conductances of the present MTJs, which provides key information to understand the mechanism of the TMR effect. Let us first focus on the Co/SrTiO₃/Co(111) MTJ with a higher TMR ratio [Figs. 3(a)–3(c)]. In the down-spin conductance $G_{P,\downarrow}(\mathbf{k}_{\parallel})$ in Fig. 3(b), one can see a smooth peak centered at $\mathbf{k}_{\parallel} = (0, 0) = \Gamma$. This reminds us of the similar peak in Fe/MgO/Fe(001) [1,2], which was explained by the coherent tunneling of the Δ_1 state at $\mathbf{k}_{\parallel} = \Gamma$. In Fig. 3(a), the up-spin conductance $G_{P,\uparrow}(\mathbf{k}_{\parallel})$ has a spikelike structure distributed circularly around the Γ point. Such a feature is often seen in other MTJs and is known to come from the interfacial resonant tunneling. In the antiparallel magnetization state [Fig. 3(c)], the \mathbf{k}_{\parallel} dependence of the conductance is like a mixture of $G_{P,\uparrow}(\mathbf{k}_{\parallel})$ [Fig. 3(a)] and $G_{P,\downarrow}(\mathbf{k}_{\parallel})$ [Fig. 3(b)] but the value of the conductance is small in each \mathbf{k}_{\parallel} point, because of the mismatch of the conductive channels between the left and right electrodes. The \mathbf{k}_{\parallel} dependences of conductances in the Ni-based MTJ [Figs. 3(d)–3(f)] are almost similar to those of the Co-based MTJ. A minor difference is that the peak in the down-spin conductance [Fig. 3(e)] is not so smooth compared to that of the Co-based MTJ. However, the similarity in the \mathbf{k}_{\parallel} -dependent conductances indicates that the TMR effects in these MTJs can be explained by the same mechanism.

Let us discuss the mechanism of the TMR effect on the basis of the electronic structures of the tunnel barrier and ferromagnetic electrodes. We mainly focus on the Co/SrTiO₃/Co(111) MTJ, since the similar mechanism is expected for both the MTJs. As mentioned above, the smooth peak in the \mathbf{k}_{\parallel} -dependent conductance [Fig. 3(b)] reminds us of the well-known coherent tunneling mechanism, in which bulk band structures of the tunnel barrier and ferromagnetic electrodes along the k_z line at the Γ point can explain a high TMR ratio. In the conventional (001)-oriented MTJs, such a high symmetry line in the Brillouin zone is called the Δ line. On the other hand, in the present (111)-oriented MTJs, the Λ line corresponding to the [111] direction plays the key role for the coherent tunneling.

Figure 4(a) shows real and complex band structures of SrTiO₃ along the Λ line. Here, the Fermi level E_F is set to that of SrTiO₃ attached to Co, which was estimated by the Co/SrTiO₃/Co(111) supercell. Around $E = E_F$, the real band has an insulating gap of ~ 1.04 eV, which is smaller than the typical theoretical value in SrTiO₃ (~ 1.9 eV) estimated by similar first-principles calculations [24,25]. This is because the in-plane lattice constant of SrTiO₃ is shrunk so as to fit that of fcc Co and the tensile strain ($\sim 23\%$) is applied along the [111] direction. Because of such a small band gap in SrTiO₃, the present MTJs have small values of resistance-area product (RA), which are beneficial for realizing read sensors of high-density hard disk drives and Gbit-class magnetic random access memories. By calculating the inverse of G_P/A in Table II, we obtained RA of 6.52 and 26.46 $\Omega \mu\text{m}^2$ in the Co- and Ni-based MTJs, respectively. These values are much smaller than that in the typical Fe/MgO/Fe(001) MTJ with a similar barrier thickness ($\sim 10^3 \Omega \mu\text{m}^2$) [see Fig. 4(b) of Ref. [26]].

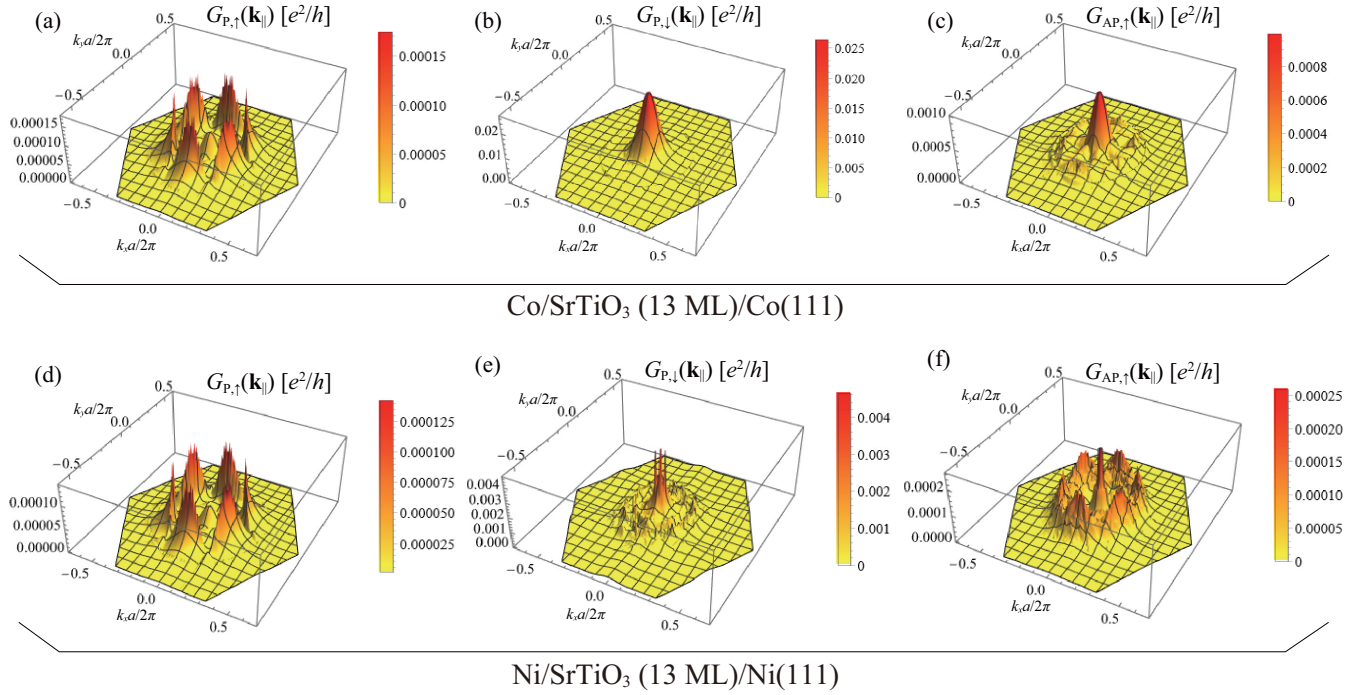


FIG. 3. \mathbf{k}_{\parallel} -dependent conductances in Co/SrTiO₃ (13 ML)/Co(111) [(a)–(c)] and Ni/SrTiO₃ (13 ML)/Ni(111) [(d)–(f)], where $\mathbf{k}_{\parallel} = (k_x, k_y)$ is given in the Cartesian coordinates. (a),(d) Up-spin conductances $G_{P,\uparrow}(\mathbf{k}_{\parallel})$ and (b),(e) down-spin conductances $G_{P,\downarrow}(\mathbf{k}_{\parallel})$ in the parallel magnetization configurations. (c),(f) Up-spin conductances $G_{AP,\uparrow}(\mathbf{k}_{\parallel})$ in the antiparallel magnetization configurations.

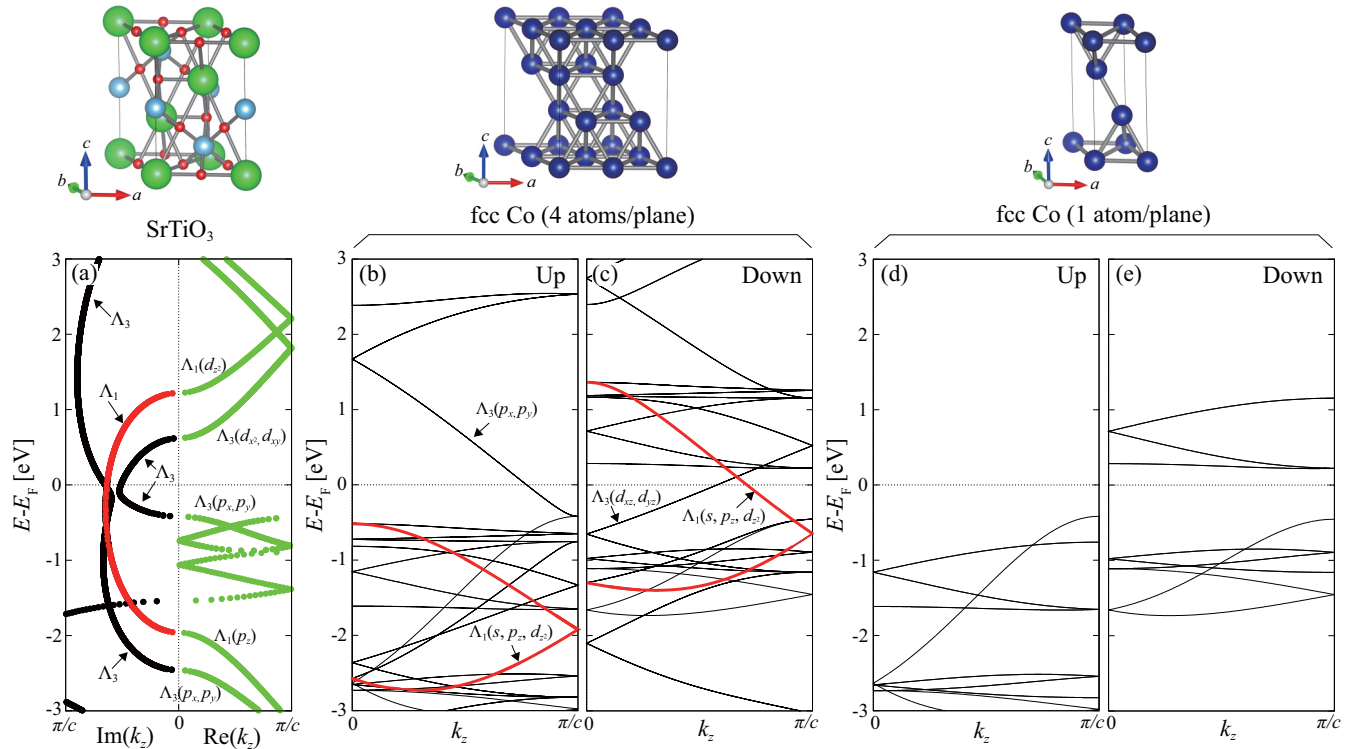


FIG. 4. (a) Real and complex band structures along the Λ line of SrTiO₃. (b) Up-spin and (c) down-spin band structures along the Λ line of fcc Co calculated for the unit cell with four atoms in each plane. In (a)–(c), the irreducible representation and atomic orbitals contributing dominantly to each band are indicated, where $d_{3z^2-r^2}$ and $d_{x^2-y^2}$ are abbreviated as d_{z^2} and d_{x^2} , respectively. (d),(e) The same as (b),(c) but for unit cell with one atom in each plane. The unit cells used in the calculations are also shown.

In Fig. 4(a), three complex bands cross $E = E_F$, where one of them has Λ_1 symmetry (red curve) and the others have Λ_3 symmetry (black curves). The s , p_z , and $d_{3z^2-r^2}$ orbitals rotationally symmetric along the [111] direction belong to the Λ_1 state and the other p and d orbitals belong to the Λ_3 state. Note here that $\text{Im}(k_z)$ provides a decay rate of the wave function in the barrier layer. Since all three complex bands have similar values of $\text{Im}(k_z)$ at $E = E_F$, both Λ_1 and Λ_3 wave functions of the electrode are expected to decay with a similar length scale in the SrTiO₃ barrier.

We next calculated the band structure of fcc Co along the Λ line as shown in Figs. 4(b) and 4(c), using the unit cell extracted from the Co/SrTiO₃/Co(111) supercell. One can find the half-metallic nature in the Λ_1 state (red curves); namely, the Λ_1 band in the down-spin state crosses E_F , while that in the up-spin state does not cross E_F . The relatively high TMR ratio in this system is attributed to the coherent tunneling of the half-metallic Λ_1 state. However, the TMR ratio (534%) is lower than that of the conventional Fe/MgO/Fe(001) MTJ (>1000%) with a half-metallic Δ_1 state in Fe [1,2]. As shown in Figs. 4(b) and 4(c), the Λ_3 band crosses E_F in both up- and down-spin states. Since the Λ_3 state has a similar decay rate as the Λ_1 state [Fig. 4(a)], these up- and down-spin Λ_3 bands enhance the conductance G_{AP} and thus decrease the TMR ratio. We also analyzed the band structure of fcc Ni in Ni/SrTiO₃/Ni(111) and found a similar half-metallic nature in the Λ_1 state (not shown). Thus the TMR effect in the Ni-based MTJ can also be understood by the Λ_1 coherent tunneling, even though the TMR ratio is not so high compared to that of the Co-based MTJ. The origin of such a difference will be discussed later.

Note here that the half-metallic band structure in the Λ_1 state [Figs. 4(b) and 4(c)] can be interpreted as a result of the band folding in the k_x - k_y plane. To discuss this, let us consider the primitive unit cell of (111)-oriented fcc Co shown on top of Figs. 4(d) and 4(e), which has one Co atom in each ab -plane layer and fits a simpler tunnel barrier with a smaller in-plane area like MgO. Using this unit cell, we calculated up- and down-spin band structures along the Λ line shown in Figs. 4(d) and 4(e). It is seen that no band crosses E_F in both spin states, i.e., there is no Λ_1 state at E_F . In the case of the larger unit cell that fits SrTiO₃ shown on top of Figs. 4(b) and 4(c), the a - and b -axis lengths are twice as long as those of the primitive cell and each ab -plane layer has four Co atoms. Therefore, the band structures of this extended cell are identical to those obtained by folding the band structures of the primitive cell in the k_x - k_y plane. Actually, by comparing Figs. 4(b), 4(c), 4(d), and 4(e), we see that the band folding provides additional bands crossing E_F , leading to the half metallicity in the Λ_1 state. We emphasize that this is in sharp contrast to the band-folding effect in Fe/MgAl₂O₄/Fe(001) [10–14]; the band folding gives an additional minority-spin band in the Δ_1 state of Fe, which breaks the Δ_1 half metallicity and lowers a TMR ratio. In our previous study [5], we studied the TMR effect in Co/MgO/Co(111). In this case of MgO(111), as mentioned above, the bulk band structure of Co has no Λ_1 state at E_F and cannot contribute to a high TMR ratio. Instead, in this system, we showed that the characteristic interfacial state gives a high TMR ratio through the resonant tunneling [27]. However, such

TABLE III. Conductances per unit areas and TMR ratios calculated for Co/SrTiO₃(n ML)/Co(111) ($n = 7, 13$). The units are in $\Omega^{-1}\mu\text{m}^{-2}$ and %, respectively.

SrTiO ₃ thickness	7 ML (11 Å)	13 ML (19 Å)
G_P/A	7.46	1.53×10^{-1}
G_{AP}/A	2.20	2.42×10^{-2}
TMR ratio	240	534

a high TMR ratio might be fragile against interfacial defects or impurities as mentioned in Sec. I. In contrast, the presently obtained high TMR ratio is owing to the Λ_1 half metallicity in the bulk electronic state and is expected to be more robust against interfacial imperfections than the interface-driven high TMR ratio.

The above mentioned coherent tunneling scenario of the Λ_1 state is also supported by the SrTiO₃ thickness dependence of conductances and the TMR ratio. We additionally calculated these quantities in the Co/SrTiO₃(7 ML)/Co(111) MTJ and compared them with those in the original Co/SrTiO₃(13 ML)/Co(111) MTJ as shown in Table III. We see that the TMR ratio increases with increasing the SrTiO₃ thickness. This is because the selective transport of the Λ_1 state becomes more prominent as the barrier thickness increases. A similar behavior is also seen in Fe/MgO/Fe(001) [1,2], where the TMR effect originates from the selective transport of the Δ_1 state. The decay of the parallel conductance G_P/A can be roughly estimated from the complex band shown in Fig. 4(a). When we use $\kappa = \text{Im}(k_z) = 0.6\pi/c$ as the complex wave vector for the Λ_1 state, the decay factor of the conductance is calculated as $\exp(-2\kappa d) \approx 1.86 \times 10^{-2}$, where we used $d = 8$ Å as the increment in the SrTiO₃ thickness (7 → 13 ML) and $c = 7.57$ Å as the c -axis length of the SrTiO₃ cell. Using this factor and G_P/A for 7 ML SrTiO₃, G_P/A for 13 ML SrTiO₃ is approximately estimated as G_P/A (7 ML SrTiO₃) $\times \exp(-2\kappa d) \approx 1.39 \times 10^{-1} \Omega^{-1}\mu\text{m}^{-2}$, which is close to $1.53 \times 10^{-6} \Omega^{-1}\mu\text{m}^{-2}$ (Table III) obtained in the actual transport calculation. All these results on the SrTiO₃ thickness dependence indicate that the coherent tunneling of the Λ_1 state driven by the band folding provides the dominant contribution to the TMR effect in the present systems.

We finally address the difference in the TMR ratio between the Co- and Ni-based MTJs. As mentioned above, since both Co and Ni in the present MTJs have the Λ_1 half metallicity, a more detailed comparison of the electronic structure is required. Here, we focus on the weight of the s -orbital component in the Λ_1 band, since the s -orbital state contributes dominantly to transport properties including the TMR effect owing to its small effective mass. Such a significance of the s -orbital state on the TMR effect has been reported in many previous studies [14,28–30]. Figures 5(a) and 5(b) show the down-spin band structures of Co and Ni, respectively, where the relative weight of the s -orbital component is indicated as the linewidth of each band using color. We find that the main Λ_1 band crossing E_F in Co has more s -orbital weight around E_F than in Ni. This larger s -orbital component at E_F can provide a larger conductance; in fact, as shown in Table II, the down-spin conductance $G_{P,\downarrow}$ in the Co-based MTJ is more

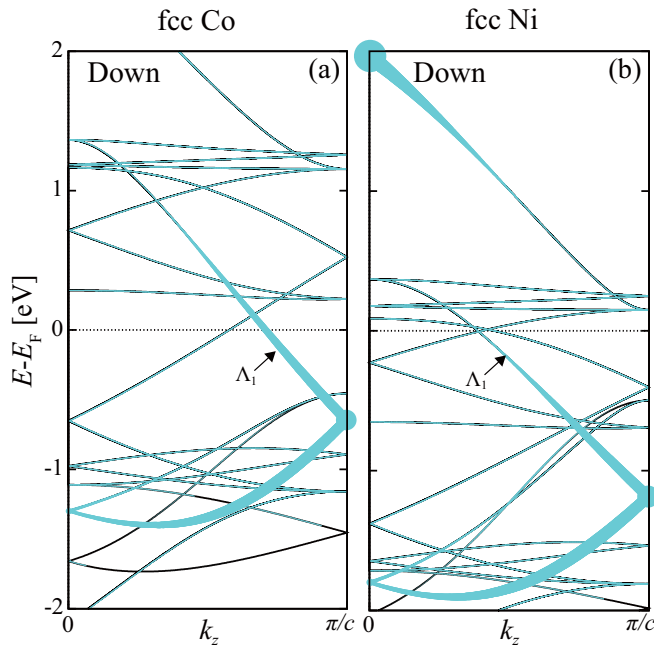


FIG. 5. Down-spin band structure along the Δ line of (a) fcc Co and (b) fcc Ni with s -orbital projection. The relative weight of the s -orbital component is indicated as the linewidth of each band using color.

than four times larger than that in the Ni-based MTJ, while the up-spin conductance $G_{P,\uparrow}$ is almost similar for both MTJs. These results indicate that a higher TMR ratio in the Co-based MTJ is attributed to a larger s -orbital component at E_F in the Δ_1 band of Co.

IV. SUMMARY

We investigated the TMR effect in unconventional (111)-oriented MTJs with SrTiO₃ tunnel barriers by means of the first-principles calculation and the Landauer formula. We obtained relatively high TMR ratios of 534 and 290% in Co/SrTiO₃/Co(111) and Ni/SrTiO₃/Ni(111), respectively.

The analysis of the bulk band structure in the electrode and the barrier regions of the MTJ clarified that the TMR effect in the present MTJs can be explained by the coherent tunneling of electronic states of bulk ferromagnets; actually, we found that fcc Co and Ni in the MTJs have half-metallic band structures in the Δ_1 state and these half-metallic states transmit through SrTiO₃ with an evanescent Δ_1 state, leading to relatively high TMR ratios. A usual primitive cell of fcc Co (Ni) has no Δ_1 state at E_F . However, since the in-plane lattice constant of SrTiO₃ is about twice as long as that of fcc Co (Ni), the 2×2 in-plane cell of fcc Co (Ni) fit the unit cell of SrTiO₃. This yields a band folding in fcc Co (Ni) in the k_x - k_y plane and the folded bands give a half metallicity in the Δ_1 state. Therefore, we can conclude that the band folding is the key for the Δ_1 half metallicity and resultant high TMR ratios. We also discussed the difference in the TMR ratio between the Co- and Ni-based MTJs and found that this is attributed to the different weights of the s -orbital component in the Δ_1 band at the Fermi level. Unfortunately, the TMR ratios of the present MTJs are not so high compared to that of the conventional Fe/MgO/Fe(001). This is because SrTiO₃ has a slow-decaying evanescent state with Δ_3 symmetry, as well as that with Δ_1 symmetry. Since fcc Co (Ni) has both up- and down-spin Δ_3 bands at E_F , these bands degrade a TMR ratio by increasing the conductance in the antiparallel magnetization state. Therefore, finding ferromagnetic materials that have a half metallicity not only in the Δ_1 state but also in the Δ_3 state is required for obtaining a giant TMR ratio in the (111)-oriented MTJs with SrTiO₃ barriers.

ACKNOWLEDGMENTS

This work was partly supported by Grants-in-Aid for Scientific Research (S) (Grant No. JP22H04966), Scientific Research (B) (Grants No. JP20H02190 and No. JP21H01750), and for Early-Career Scientists (Grant No. JP20K14782) from JSPS KAKENHI. This work was also supported by JST CREST “Integrated Devices and Systems Utilized by Information Carriers” (Grant No. JPMJCR21C1) and the Cooperative Research Project Program of the Research Institute of Electrical Communication, Tohoku University. The crystal structures were visualized using VESTA [31].

- [1] W. H. Butler, X.-G. Zhang, T. C. Schulthess, and J. M. MacLaren, *Phys. Rev. B* **63**, 054416 (2001).
- [2] J. Mathon and A. Umerski, *Phys. Rev. B* **63**, 220403 (2001).
- [3] S. Yuasa, T. Nagahama, A. Fukushima, Y. Suzuki, and K. Ando, *Nat. Mater.* **3**, 868 (2004).
- [4] S. S. P. Parkin, C. Kaiser, A. Panchula, P. M. Rice, B. Hughes, M. Samant, and S.-H. Yang, *Nat. Mater.* **3**, 862 (2004).
- [5] K. Masuda, H. Itoh, and Y. Miura, *Phys. Rev. B* **101**, 144404 (2020).
- [6] K. Masuda, H. Itoh, Y. Sonobe, H. Sukegawa, S. Mitani, and Y. Miura, *Phys. Rev. B* **103**, 064427 (2021).
- [7] J. M. De Teresa, A. Barthélemy, A. Fert, J. P. Contour, R. Lyonnet, F. Montaigne, P. Seneor, and A. Vaurès, *Phys. Rev. Lett.* **82**, 4288 (1999).
- [8] J. M. De Teresa, A. Barthélemy, A. Fert, J. P. Contour, F. Montaigne, and P. Seneor, *Science* **286**, 507 (1999).
- [9] J. P. Velev, K. D. Belashchenko, D. A. Stewart, M. van Schilfgaarde, S. S. Jaswal, and E. Y. Tsybmal, *Phys. Rev. Lett.* **95**, 216601 (2005).
- [10] Y. Miura, S. Muramoto, K. Abe, and M. Shirai, *Phys. Rev. B* **86**, 024426 (2012).
- [11] H. Sukegawa, Y. Miura, S. Muramoto, S. Mitani, T. Niizeki, T. Ohkubo, K. Abe, M. Shirai, K. Inomata, and K. Hono, *Phys. Rev. B* **86**, 184401 (2012).
- [12] K. Masuda and Y. Miura, *Phys. Rev. B* **96**, 054428 (2017).
- [13] K. Nawa, K. Masuda, and Y. Miura, *Phys. Rev. B* **102**, 144423 (2020).

- [14] K. Nawa, K. Masuda, and Y. Miura, *Phys. Rev. Appl.* **16**, 044037 (2021).
- [15] Here, the barrier thickness is defined as the distance between two ferromagnetic layers closest to the SrTiO₃ barrier.
- [16] G. Kresse and J. Furthmüller, *Phys. Rev. B* **54**, 11169 (1996).
- [17] J. P. Perdew, K. Burke, and M. Ernzerhof, *Phys. Rev. Lett.* **77**, 3865 (1996).
- [18] P. E. Blöchl, *Phys. Rev. B* **50**, 17953 (1994).
- [19] G. Kresse and D. Joubert, *Phys. Rev. B* **59**, 1758 (1999).
- [20] A. Smogunov, A. Dal Corso, and E. Tosatti, *Phys. Rev. B* **70**, 045417 (2004).
- [21] S. Baroni, A. Dal Corso, S. de Gironcoli, and P. Giannozzi, <http://www.pwscf.org>.
- [22] A. Dal Corso, *Comput. Mater. Sci.* **95**, 337 (2014).
- [23] H. Joon Choi and J. Ihm, *Phys. Rev. B* **59**, 2267 (1999).
- [24] T. Tanaka, K. Matsunaga, Y. Ikuhara, and T. Yamamoto, *Phys. Rev. B* **68**, 205213 (2003).
- [25] G. Kang, Y. Kang, and S. Han, *Phys. Rev. B* **91**, 155141 (2015).
- [26] K. Masuda and Y. Miura, *Jpn. J. Appl. Phys.* **56**, 020306 (2017).
- [27] In our previous work [5], we used a Co/MgO/Co(111) unit cell, which includes two Co atoms in each *ab*-plane layer of ferromagnetic electrodes and has a larger in-plane area than that of the primitive cell. However, both unit cells should of course give the same results. Our recent calculation using the primitive Co/MgO/Co(111) cell obtained a similarly high TMR ratio due to the interface resonant tunneling.
- [28] G.-F. Li, Y. Honda, H.-X. Liu, K.-I. Matsuda, M. Arita, T. Uemura, M. Yamamoto, Y. Miura, M. Shirai, T. Saito, F. Shi, and P. M. Voyles, *Phys. Rev. B* **89**, 014428 (2014).
- [29] K. Moges, Y. Honda, H. X. Liu, T. Uemura, M. Yamamoto, Y. Miura, and M. Shirai, *Phys. Rev. B* **93**, 134403 (2016).
- [30] K. Masuda, T. Tadano, and Y. Miura, *Phys. Rev. B* **104**, L180403 (2021).
- [31] K. Momma and F. Izumi, *J. Appl. Crystallogr.* **44**, 1272 (2011).